

Mesoscale convective systems and critical clusters

OLE PETERS *

DEPARTMENT OF ATMOSPHERIC AND OCEANIC SCIENCES
AND INSTITUTE OF GEOPHYSICS AND PLANETARY PHYSICS,
UNIVERSITY OF CALIFORNIA, LOS ANGELES, USA.

J. DAVID NEELIN

DEPARTMENT OF ATMOSPHERIC AND OCEANIC SCIENCES
AND INSTITUTE OF GEOPHYSICS AND PLANETARY PHYSICS,
UNIVERSITY OF CALIFORNIA, LOS ANGELES, USA.

STEPHEN W. NESBITT

DEPARTMENT OF ATMOSPHERIC SCIENCES
UNIVERSITY OF ILLINOIS AT URBANA-CHAMPAIGN, IL, USA.

* *Corresponding author address:* Ole Peters, 405 Hilgard Ave., Los Angeles, California 90095-1565, USA.

ABSTRACT

Size distributions and other geometric properties of mesoscale convective systems (MCS), identified as clusters of adjacent pixels exceeding a precipitation threshold in satellite radar images, are examined with respect to a recently identified critical range of water vapor. Satellite microwave estimates of column water vapor and precipitation show that the onset of convection and precipitation in the tropics can be described as a phase transition, where the rain rate and likelihood of rainfall suddenly increase as a function of water vapor. This is confirmed in Tropical Rainfall Measuring Mission radar data used here. As is known from percolation theory, cluster properties are highly sensitive to changes in the rainfall probability, and thereby to changes in the water vapor. To confirm this we categorize clusters by their prevalent water vapor. As expected, mean cluster size and radius of gyration strongly increase as the critical water vapor is approached from below. In the critical region we find scale-free size distributions spanning several orders of magnitude. Large clusters are typically from the critical region: at low water vapor most clusters are small, and super-critical water vapor values are too rare to contribute much. The perimeter of the clusters confirms previous observations in field- and model-data of robust non-trivial scaling. The well-known area-perimeter scaling is fully compatible with the quantitative prediction from the plausible null-model of gradient percolation, where the accessible hull is a fractal object with dimension $4/3$.

1. Introduction

Mesoscale convective systems (MCSs) have been the object of much study due to their importance for severe weather and rainfall production (Cotton and Anthes 1989; Houze 2004). One common tool in studying these systems has been to examine clusters of connected pixels for radar, microwave or infrared indicators of cloud. Working definitions of MCSs are phrased in terms of such clusters; *e.g.* an area of brightness temperature below 250 K of at least 2000 km² (Mohr and Zipser 1996), or a linear dimension of at least 100 km in one direction (Houze 1993; ?; Nesbitt et al. 2006) (plus the widely met criterion of strong convection within the cluster). The size distribution of these clusters has often been described as lognormal (López 1977; Houze and Cheng 1977; Cheng and Houze 1979; Williams and Houze 1987; Houze 1993) (where “size” refers to the horizontal area) although recent data (Mapes and Houze 1993; Nesbitt et al. 2006) indicate that the correspondence to lognormal is rather loose. We will use the term “precipitation cluster” for any collection of adjacent radar pixels indicating precipitation, since the clusters discussed do not all meet the traditional size criterion for MCS.

Recently Peters and Neelin (2006) (PN hereafter) noted that the transition to strong precipitation in the tropics exhibits properties of non-equilibrium continuous phase transitions for which there exists an extensive literature (see review by Hinrichsen 2000). Using TMI data for column integrated water vapor and microwave estimated precipitation (Wentz and Spencer 1998), they showed a sharp increase in precipitation above a critical value of the water vapor. The functional form of the increase above criticality was consistent with a power law. In the parlance of continuous phase transitions, the water vapor was interpreted

as a tuning parameter and the precipitation rate as an order parameter. Near criticality the variance of the order parameter (a measure of thermodynamic susceptibility) was found to peak strongly, and a finite-size scaling analysis revealed long-range (power law) correlations in the precipitation field, all in agreement with the theory of continuous phase transitions. We will refer to this transition as the precipitation transition for brevity, with the understanding that in cases studied here the transition is associated with the transition to strong deep convection.

The fact that long-range spatial correlation persisted over the observed spectrum of scales (up to several hundred km) suggests that spatially structured objects exist at least up to this scale. Meteorologically, PN suggested that these objects are likely to correspond to MCSs, relating them to critical clusters in other systems (Stauffer and Aharony 1994). Here we seek to confirm and quantify a change in properties of tropical mesoscale convective clusters associated with the precipitation transition identified in PN, using Tropical Rainfall Measuring Mission (TRMM) 2A25 radar data and the cluster algorithm of Nesbitt et al. (2006), for which the mesoscale cluster properties have already been established with respect to traditional mesoscale meteorological approaches. From the mesoscale modeling literature, there are indications that tropospheric water vapor can affect tropical rainfall characteristics in general Bretherton et al. (2004), and in particular MCSs (Lucas et al. 2000; Tompkins 2001), with some support in conventional observational diagnostics (LeMone et al. 1998). Given the strong dependence of rainfall probability on water vapor and the expected sensitive dependence of cluster properties on rainfall probability, we anticipate a change in cluster properties as the water vapor crosses the critical point.

Thermodynamic issues are commonly discussed in terms of geometric properties of spatial

domains. For example, the critical behavior of the Ising model, a mathematical caricature of a ferromagnet, can be formulated in terms of geometric properties of clusters of aligned spins. Its free energy functional can be written as a summation over different configurations of domain walls (Cardy 2005). For an introductory review see Ch. 7 of Stauffer and Aharony (1994). From this literature we extract the caveat that certain geometric properties (for instance area-perimeter scaling, see below) are so robust that they are insensitive to the physical processes that generate them. These properties can easily be predicted, but they tell us little about the physics behind them. Whenever spatial clusters are important in the statistical description of a system, a comparison to the null-model of spatial clustering, percolation, is worthwhile. In the present context we have to deal with the added difficulty of inhomogeneity, both in water vapor (here measured by the column integrated water vapor $w(\mathbf{x}, t)$) and in the resulting rain field. The lessons from percolation theory will therefore be largely reduced to qualitative statements. These do, however, set hypotheses for the behavior of precipitation cluster statistics as a function of water vapor, which we can then test.

Before we describe the set-up of percolation, we note its importance here not only as an extremely simple model of spatial clustering but also as an extremely simple model with a continuous phase transition. We first recap geometric properties that are of interest for our study and then discuss the limitations of the comparison between MCSs and percolation clusters.

In its simplest form, percolation theory is concerned with uncorrelated lattice sites, all of which are occupied with a probability p (Stauffer and Aharony 1994). At low concentration of occupied sites, clusters are typically small, and large agglomerations are exponentially

unlikely. As p is increased, however, typical cluster sizes grow until the critical point is reached, $p = p_c$, where percolation occurs: In a system whose linear size, L , approaches infinity, a cluster spans the system, providing paths of occupied nearest-neighbor sites between opposing system boundaries. In the thermodynamic limit, $L \rightarrow \infty$, the average cluster size $\langle s \rangle (p)$ diverges as a power law as p_c is approached,

$$\lim_{p \rightarrow p_c} \langle s \rangle (p) = a_s^\pm |p - p_c|^{-\gamma}, \quad (1)$$

where a_s^\pm denotes the proportionality factors for $p < p_c$ and $p > p_c$. The average radius of gyration, $\langle r \rangle (p)$ diverges similarly,

$$\lim_{p \rightarrow p_c} \langle r \rangle (p) = a_r^\pm |p - p_c|^{-\nu}. \quad (2)$$

The ensemble considered for the averages does not include any spanning clusters (clusters that connect opposing system boundaries). Including such clusters, the average cluster size would tend to infinity for $p \geq p_c$ in the thermodynamic limit. The factors a_s^\pm and a_r^\pm are non-universal, *i.e.* they depend on microscopic details like the lattice structure (triangular, hexagonal, square...). The exponent γ (as well as amplitude ratios, such as $\frac{a_r^+}{a_s^+}$), on the other hand, are universal to all percolation systems, depending only on the dimensionality of the lattice. For finite systems at criticality, the distribution of cluster sizes is cut off at an L -dependent characteristic size $s_\xi \propto L^D$, which dominates the average cluster size. The divergences Eq. (1) and Eq. (2) are then capped, since there cannot be an infinite cluster in a finite system.

The size distribution of clusters at the critical point p_c is scale-free,

$$n_s(s; L) = s^{-\tau} \mathcal{G}(s/s_\xi), \quad (3)$$

where $n_s(s)$ denotes the “cluster number”, or probability density of a given cluster having size s . In finite systems, the cluster size distribution is cut off by a scaling function $\mathcal{G}(s/s_\xi)$ with the single argument s/s_ξ . Clusters larger than the characteristic size s_ξ are extremely unlikely, $\forall n, \lim_{s \rightarrow \infty} s^n G(s/s_\xi) = 0$. This expression simply means that none of the moments of the size distribution diverge, which is necessarily true for any finite system. The function $\mathcal{G}(x)$ is further required to be infinitely differentiable and be constant for small arguments, $\lim_{x \rightarrow 0} \mathcal{G}(x) = \text{const}$. In the thermodynamic limit one thus recovers the pure power-law behavior. As s_ξ diverges, the argument $x = s/s_\xi$ approaches zero, and $n_s(s) = \text{const} \times s^{-\tau}$. Otherwise $\mathcal{G}(x)$ is *a priori* quite arbitrary and can take various shapes, depending, *e.g.* on the aspect ratio of the system (Moloney and Pruessner 2003).

The critical exponents γ, ν and τ are universal to all two-dimensional percolation problems. In practice we observe (from small to large clusters) a distribution that starts out fairly arbitrary, then follows a power law over a range that depends on the system size and finally decays very fast, for example like an exponential. For this reason, the “true” (infinite-system) behavior of $n_s(s)$ is sometimes difficult to infer from observations. For example, the universal exponent τ can in principle be read off a double-logarithmic plot as the negative slope in the power-law regime. However, the change from the power-law regime to the cut-off regime is often gradual, which can produce a continuously changing slope, making it impossible to ascribe a single value to the exponent. To address these problems systematically, a finite-size scaling analysis would be required, where the system size is changed in a controlled way and the spatial structure of $p(\mathbf{x})$ is known precisely. This, however, is beyond the scope of the present paper.

In studies of clusters in continuous phase transitions (like the percolation transition), the

tuning field that controls the phase transition (in percolation $p(\mathbf{x})$) is usually homogeneous in space. In a field with strong inhomogeneities, such as the environment that controls the emergence of precipitation clusters (or MCSs), we can only expect the most robust homogeneous properties to survive. For example, we mentioned that system-spanning clusters are removed from any averages. Above percolation-criticality only small clusters occur in the holes of the infinite (or spanning) cluster. The infinite cluster has a very small density near the phase transition, and many holes exist. In the case of precipitation clusters, however, we expect meteorologically that the interior of a cluster is quite dense. Clusters from the holes of other clusters therefore contribute negligibly to the statistics. Furthermore, while we remove clusters that span the radar swath, spanning criteria that take into account the inhomogeneities have not been developed, for instance, one could remove clusters that span a region of elevated water vapor. The super-critical behavior of Eq. (1) is thus not expected to be reproduced – while approaching the transition from below, the average cluster size will sharply increase, it is unlikely to decrease above criticality.

We can make a very robust prediction about MCS-perimeters based on a set-up called gradient percolation (Gouyet and Rosso 2005). Consider a two-dimensional system of length L whose occupation probability is a function of one spatial coordinate. It is fully occupied at one end, $p(0, y) = 1$, from where the occupation probability decreases linearly in x to $p(L, y) = 0$. Clearly, there will be a cluster connecting the bottom ($y = 0$) to the top ($y = L$) at $x = 0$. There will certainly be no such cluster at $x = L$ where the occupation probability is zero. Somewhere in between there must therefore be a boundary, called the hull, of the cluster that spans from top to bottom. The fractal dimension of this boundary depends on the precise definition of the hull. For the most robust object (Kolb 1990), which is

known as the “accessible hull”, it is $d_f = 4/3$. In the present context it is important that the hull was identified on a length scale (the pixel size) that is larger than the fundamental scale of the processes generating the cluster. The spatial resolution of the TRMM precipitation radar of about 5 km is not fine enough to capture all the details of the cluster. The perimeter measured on this scale corresponds to the accessible hull (as opposed to the full hull). The difference between the hull and the accessible hull was first pointed out by Grossman and Aharony (1986). Without discussing the issue in detail we note that it is counter-intuitive for a scaling-property like the hull dimension to depend on the microscopic details of the hull-definition. This aspect has been treated in the mathematical physics literature and is now well understood. The full hull (whose dimension is $7/4$) would only be observed for extremely large clusters that are certainly beyond the size-limit imposed by the inhomogeneity of the vapor field and the scales investigated here. The robustness of this prediction can be understood as follows: While other quantitative results crucially depend on a good estimate of the relevant occupation probability p in the environment that a given cluster inhabits, this is not the case for the hull dimension. As long as the spatial dependence of p can be linearized in the vicinity of the perimeter, the result holds. The precise morphology of the clusters is thus not important – instead of a gradient along one dimension, this would apply for an MCS that is healthy (high p) in the center, with conditions becoming progressively less favorable (decreasing p) as one moves out to the surrounding environment. An explicit measurement of $p(\mathbf{x})$ is not required.

Apart from the very robust exponent just described, we do not attempt to relate apparent exponents to specific models or processes. This would require knowledge of the spatial structure of any inferred precipitation probability p .

Above the critical water vapor, w_c , not only the average rain intensity increases sharply but also the probability of observing 20 dBZ radar reflectivity. With respect to clusters of precipitating pixels, this is akin to the occupation probability p in percolation problems. Geometric critical phenomena of the type described above will occur near w_c (because p changes quickly here), with the precise point in w determined by the particular cut-off value for considering a pixel as precipitating (here 20 dBZ). If the convective and geometric critical points do not occur at precisely the same value of water vapor, then much of the observed geometric behavior will be unaffected by the physical processes. This has the advantage that geometric properties of rainfields can be understood without knowledge of precipitation physics, but it has the disadvantage that geometric properties have little discriminative power with respect to physical processes.

2. Data and methods

Version 6 TRMM precipitation radar (PR) data from algorithm 2A25 (Iguchi et al. 2000) from 1 January 1998 through 31 December 2006 was used in the present analysis. A modified version of the algorithm described by Nesbitt et al. (2006) was used to identify precipitation features – clusters of contiguous pixels exceeding a given reflectivity. The modifications are (i) only the PR Near Surface Reflectivity field was used to identify contiguous pixels > 20 dBZ (no microwave imager data were used in the grouping), and (ii) next-nearest-neighbor pixels were not included in the feature grouping (i.e. only adjacent pixels were included). The latter modification was done to match common practice in the percolation literature (Stauffer and Aharony 1994). For each identified feature, the area, accessible hull

length, and radius of gyration were computed. The area of each feature was calculated by summing the number of pixels and multiplying by the nominal PR instrument field of view ($(4.23 \text{ km})^2/(4.51 \text{ km})^2$ before/after 8 Aug 2001). These values were computed as the mean area projected by the PR pixel centroids as if it were a square lattice. The hull length was calculated by walking along the edges of all boundary pixels of a given feature in counterclockwise direction, summing the distance traveled until the starting point is reached. Accessible hull length is calculated a similar way, except gaps less than one pixel in width are treated as cells on the feature boundary. Long fjords into the features are thereby cut off. The radius was computed as described below, see Eq. 7. Each cluster was associated with the precipitable water value from the TMI pixel that contains the cluster centroid. The TMI resolution is about 25 km, compared to the radar’s approximately 5 km, so this samples a square of about 25 radar pixels characterizing the interior environment for large clusters, with the caveat for small clusters that some exterior environment is inevitably sampled as well. This “centroid-surrounding value” seems the most appropriate choice, within the resolution limitations. The cluster statistics are then binned for each 1 mm interval in water vapor. For removal of spanning clusters, we have implemented the criterion of spanning the radar swath (215 km/247 km wide before/after 1 August 2001), which would be appropriate in a homogeneous water vapor environment, with caveats discussed below. In Fig. 3, 4, 6, and 7 swath-spanning clusters were removed but clusters touching one side of the swath were left in the ensemble. The restrictions on data in Fig. 5 and 8 are even stricter: boundary-touching clusters are also removed since the swath would introduce artificially straight sections of accessible hull.

To compute non-geometric properties, in particular the ensemble-average radar precipi-

tation rate as a function of precipitable water, the 2A25 radar rain rates were averaged onto the TMI water-vapor grid (0.25×0.25 degrees latitude-longitude).

Following PN, all analyses were carried out for four major tropical (20°S to 20°N) ocean basins, the western Pacific (120°E – 170°W), eastern Pacific (170°W – 70°W), Atlantic (70°W – 20°E), and Indian Ocean (30°E – 120°E).

3. The precipitation transition in radar precipitation data

A first major step is to establish that the transition seen in PN in microwave precipitation retrievals is found in the radar retrievals. Specifically, we expect that above a critical value of the column water vapor w_c the ensemble average precipitation as a function of w will approach

$$\langle P \rangle (w) = a(w - w_c)^\beta \tag{4}$$

from a region of opposite curvature starting below w_c that is due to finite-size effects or effects of variables other than w . We also expect a steep drop in the frequency of occurrence of a given value of w for $w > w_c$. The power-law pick up of the precipitation above w_c in Fig. 1 shows remarkable agreement with that established from the microwave data in PN. The amplitudes of the TMI Wentz algorithm rainfall are significantly higher, which may be of interest for the comparison of rainfall algorithms, but, in the language of continuous phase transitions, such amplitudes are nonuniversal and not of primary interest from this point of view. The exponent 0.265 of the power law shown in the inset of Fig. 1 is the average of

the best-fit values for β for the different regions. We used the following fitting procedure: Choose a fitting range [$w^* : 75$]. Find the values for $w_c < w^*, \beta$ and a that minimize the χ^2 in log-log space between the data and Eq. 4. Repeating this for all possible w^* yields the minima χ_{\min}^2 as a function of w^* . Now divide each minimum by the number of terms contributing to the χ^2 -sum. This “error per data point” is a non-monotonic function for the data, and the minima indicate the best-fit values of w_c, β and a . From the differences in χ_{\min}^2 we estimate an error bar of about ± 0.04 for β . This result is compatible within error bars with the exponent estimated in PN, where $\beta = 0.215 \pm 0.02$ was found (with a slightly different algorithm). It indicates that there is no significant net effect from the processes that distinguish radar- from microwave-inferred estimates of rainfall intensity on the universal value of the power-law exponent. The radar and microwave measurements do not agree in terms of amplitudes (a in Eq. 4). The average estimated rain rate at a given water vapor above criticality is typically about 4 times larger in the TMI (Wentz and Spencer 1998, algorithm) data set. The best-fit critical values w_c are 65.6 mm, 65.7 mm, 63.2 mm, and 67.8 mm, respectively for the eastern Pacific, western Pacific, Atlantic and Indian Ocean. They agree to ± 1.9 mm with the values found in PN.

The agreement of the radar with the microwave retrievals in β and w_c has substantial implications for the physics of the precipitation transition. It implies that large hydrometeors with nonnegligible fall speeds are involved, while from the TMI retrievals the partition into rain and cloud water depended on algorithm assumptions. Figure 2 shows the frequencies of occurrence of different levels of water vapor in the investigated tropical regions. The distributions are very clearly different, reflecting climatic differences. We will argue below that cluster size distributions (just as precipitation rates) conditioned on specific levels of

water vapor have universal features. Since in many studies the cluster size distributions are effectively weighted by the non-universal distributions of water vapor, the universal properties are not observed.

4. Mean cluster size and radius of gyration

We define the mean cluster size, $\langle s \rangle (w)$ as the first moment of the observed cluster sizes s_i with corresponding binned water vapors w_i , conditioned on some value of the water vapor $w \in \{w_i\}$,

$$\langle s \rangle (w) = \frac{\sum_i s_i \delta(w_i, w)}{\sum_i \delta(w_i, w)}, \quad (5)$$

with the Kronecker delta $\delta(x, y) = 0, 1$ if $x \neq y$ and $x = y$, respectively. We express the size in km^2 . The radius of gyration r is the root-mean-square distance of (the mid-points of) all cluster sites j from the center of mass, \mathbf{x}_{CM} ,

$$\mathbf{x}_{CM} = \frac{\sum_j \mathbf{x}_j}{\sum_j 1} \quad (6)$$

$$r^2 = \frac{\sum_j |\mathbf{x}_j - \mathbf{x}_{CM}|^2}{\sum_j 1}. \quad (7)$$

The conditional average radius of gyration, $\langle r \rangle (w)$, is defined equivalently to the mean cluster size, replacing s_i by r_i in Eq. (5).

As mentioned above, these quantities are expected to increase sharply near the critical point, and indeed they do, as seen in Fig. 3 and Fig. 4. The increase in both quantities occurs at a lower water vapor in the Atlantic, roughly corresponding to the lower value of w_c in that basin. This also implies that the Atlantic statistics have larger estimation error at higher water vapor because the frequency of occurrence decreases rapidly near and above

criticality (Fig. 2). In homogeneous systems there would be a maximum at criticality since we removed from the sample any clusters spanning the radar swath. In the present (considerably inhomogeneous) system we observe large fluctuations and a slight further increase as the tuning parameter surpasses its likely critical value. The strong inhomogeneities in the w -field make the clusters more compact in the interior. Holes in which smaller clusters could live are rare and only large clusters contribute to the average. Thus the compactness of clusters can lead to a continued increase in the average cluster size above criticality. We removed spanning clusters to facilitate comparison with studies in statistical mechanics. The small effect of this procedure indicates that the inhomogeneities in the system are a stronger constraint than the the swath width.

Figure 5 supports the view that the clusters are compact objects since their gyration radius scales trivially as the square-root of the area. For a fractal object this would not be the case. It is important to point out, however, that percolation clusters are quite compact (their fractal dimension is $91/48 \approx 1.9$) and it is not possible to distinguish these two behaviors from this figure alone. The blue straight line in Fig. 5 indicates the minimum possible radius of gyration for a given cluster size – that of a perfect disk with equal area. The red line is the maximum possible radius – that of a straight line whose width is given by the pixel size. Not surprisingly, (for the 20 dBZ threshold used here which tends to include cloud shields for squall line structures) clusters are closer to being disks than lines. Very large clusters tend to be slightly elongated, which could be due to limits imposed by the swath width.

5. Water vapor dependence of cluster size distributions

Purely based on a diverging correlation length, in a system approximating a continuous phase transition we expect a range of scales that exhibit scale-free behavior near criticality – in our case, a range of convective cluster sizes distributed according to a power law.

As discussed in section 1, even for systems much simpler than the atmosphere it is a difficult task to measure the scaling behavior. To the usual complications are added potential impacts of inhomogeneity in water vapor, and the competition between properties of the purely geometric phase transition and the nearby physical precipitation transition. The physical MCSs are generated by the transition to strong convection, and one would expect the precipitation-critical point to coincide with that of percolation. However, the geometric properties examined here depend on the 20 *dBZ*-threshold, so the geometric phase transition need not occur at exactly the same point as the precipitation transition (although the rapidity of the radar pickup as a function of water vapor will tend to keep them close for reasonable choices of threshold). In PN long-range correlation, associated with the precipitation transition was found as far as 20 mm in water vapor away from criticality. Another problem is the influence of other unobserved atmospheric variables, such as tropospheric temperature, that also have an effect on the likelihood of precipitation.

Bearing this in mind, we expect to find a regime near w_c with scale-free cluster-size distributions (up to a cut-off set by swath width and water vapor inhomogeneity) and a regime well below w_c where cluster sizes decay fast beyond a characteristic size smaller than the hard limit set by the system size. The observed cluster size distributions in Fig. 6 and Fig. 7 follow these expectations. The size distribution changes dramatically as a function

of the water vapor, with the expected rapid cut off for low water vapor values and a substantial scale free range for near-critical values. Most large clusters occur at near-critical values. Super-critical w -values also generate large clusters, with the distribution dropping less steeply. However, these high w -values occur infrequently (see Fig. 2) so that the overall contribution remains relatively small. The weights of different water vapors in the overall distribution of cluster sizes can be read off Fig. 6 or Fig. 7 by comparing ranks or densities at the same area (looking up from a point on the abscissa).

For reference, the straight line corresponding to the exponent for two-dimensional critical percolation (in a homogeneous system) is included on the plot. While underlining that no fit should be claimed here, we emphasize that cluster size distributions in this respect comparable to the statistics of MCSs can be produced by a model where clustering occurs not because of dynamics but simply because a number of pixels is forced into a two-dimensional space. For the reasons discussed above we are precluded from ascribing effects fully to percolation or the physical transition. Nonetheless the fact that clusters size distributions are fat-tailed should come as no surprise when clusters from the critical region are included in the statistics.

It has been argued that in an ensemble that includes both measurements in the critical region and measurements outside that region it is possible to obtain cluster size distributions with exponents larger than the “correct” critical value (Sornette 1994) depending on the weight of measurements from the critical regime in the ensemble. Combining this with the complicated spatial structure of the water vapor field, this may affect the apparent exponent seen here, and contribute to the observed dependence on water vapor. Nonetheless, stratifying the behavior by water vapor as is done here clearly helps in distinguishing differ-

ent regimes of behavior. It is clear that attempts to infer functional forms of distributions by fitting data that combine different values of water vapor can lead to different conclusions, depending on whether a predominantly dry or moist area is being investigated. An exponential fits the distributions for low water vapor quite well, whereas broader distributions are needed for larger w -values, with a power law yielding the best fit near criticality.

6. Accessible hull scaling

Finally we examine the length of the accessible hull, h , for which we have a robust prediction from the gradient percolation prototype discussed in the introduction. Specifically, we expect the accessible hull to be a fractal with dimension $d_f = 4/3$. The accessible hull is the number of cluster sites adjacent to empty sites that can be reached from outside the cluster without having to pass through any narrow gates. We define a narrow gate as an opening no wider than one pixel. As was argued earlier, since the physical processes are not fully resolved by the data grid, a measurement of the hull without enforcing the no-narrow gates criterion is approximately equivalent to measuring the accessible hull and yields very similar results (not shown). We use the criterion here to avoid any ambiguity, remarking that we expect the distinction between hull and accessible hull be more important in studies using data with higher spatial resolution.

An easy way to test the predicted scaling is a comparison between cluster size and hull length. The cluster is dense in its interior, with few holes. The area enclosed by the accessible hull is therefore approximately the cluster size. If the hull is a fractal with dimension $4/3$,

its length, h , will scale with cluster size, s , as $h \propto \left(s^{\frac{1}{2}}\right)^{\frac{4}{3}}$. Figure 8 shows the median h as a function of $s^{\frac{1}{2}}$. The agreement with the asymptotic (large-cluster) prediction from gradient percolation is very good for clusters consisting of more than about 10 pixels. Large clusters tend to be associated with high water vapor values and a gradient of $w(\mathbf{x})$ from interior to exterior, which is another reason why gradient percolation would apply particularly well here.

Under the argument above that coarse resolution measurements of the perimeter tend to be effectively equivalent to the accessible hull, we can compare to earlier perimeter-area scaling results for clouds or clusters (with the caveat that deviation toward the full hull scaling of $7/4$ might occur at high resolution or for large clouds/clusters). Results approximately consistent with the $4/3$ scaling have been repeatedly noted over various scale ranges (Lovejoy 1982; Cahalan and Joseph 1989; Benner and Curry 1998; Mapes and Houze 1993). Lovejoy (1982) used rain and cloud areas from satellite images and explicitly noted the proximity of the measured dimension to $4/3$: “The value 1.35 is so close to the value $4/3$ [...] An understanding of the physical origins of this value could therefore be important.” Mapes and Houze (1993) give 1.4 for IR-based cloud clusters; the Cahalan and Joseph (1989) ITCZ case yields values around 1.4-1.5 and Benner and Curry (1998) note 1.37 ± 0.06 for their larger clouds. The latter two references note a scale break to smaller values at $O(1 \text{ km})$, but may be interpreted as indicating that the scaling that applies for MCSs may continue down to the scales of individual cloud plumes. Universality as in the case of the fractal dimension typically occurs in an intermediate-asymptotic regime (Barenblatt 1996), that is, on scales that are large compared to their individual components, such as

convective cells, and small compared to other constraints – such as large-scale variations in meteorological conditions. We summarize that a fractal dimension consistent with $4/3$ (with the caveat of some scatter in the estimates from various studies), in a scaling regime spanning about three orders of magnitude in linear cloud/cloud cluster size can be considered a well established observation. Recognizing this, Siebesma and Jonker (2000) confirmed that the fractal dimension is reproduced in large-eddy simulations of cumulus clouds and argued that reproducing a non-trivial scaling relation is a strong test for model validity.

Geometric measures being dominated by percolation universality rather than physical processes is widely observed in two-dimensional lattice models Fortunato (2002); Kertész (1989), and even two dimensional turbulence Bernard et al. (2006). This suggests an answer to the questions concerning the physical origins of the scaling and the discriminative power of the scaling in model testing. As in the systems cited above, the scaling for precipitation clusters appears to be dominated by geometric constraints rather than physical processes. A number of very different physical processes would produce the same value. While this may be disappointing in terms of discriminative power in model testing, it suggests that simple representations of clusters are feasible in model parameterizations.

7. Discussion

As a key starting point, we confirmed qualitatively and quantitatively in TRMM radar data properties of tropical precipitation rate versus column water vapor w that were reported for microwave-inferred rain rates in PN. These properties are consistent with those of a continuous phase transition. The power-law pick-ups of conditionally averaged precip-

itation rates as a function of water vapor exhibit critical water vapor values w_c for various tropical regions. The microwave-inferred critical values w_c^i and the power-law exponent β are compatible with the radar data.

As conjectured, the statistics of the precipitation clusters change strongly as a function of water vapor measured inside the cluster. The average size of the clusters and the average radius of gyration increase sharply near the transition point. The size distribution of precipitation clusters alters dramatically as a function of the water vapor. For low values of w the distribution decays fast for large clusters, while at very high water vapor, above the transition, the frequency of large clusters drops less quickly. The strong dependence on water vapor implies that studies of size distribution that do not account for this variable end up examining the weighted average of very different dependences. The frequency of occurrence of w (Fig. 2) does not have a universal form and can vary considerably among regions, which may provide an explanation for the different functional forms of size distributions that have been suggested in the literature. By first stratifying by w , we examined whether there is a scale-free range at w -values where theory would lead one to expect it: near the critical point of the precipitation transition – and this indeed appears to be the case. The exponent of the associated power law is sufficiently similar to that of the simplest protocol that yields such size distributions, two-dimensional percolation, that one might consider this a useful reference against which to test other hypotheses for the statistics of MCSs.

We note a number of ways in which the precipitation clusters differ from simple percolation. From the outset, we know that percolation cannot produce conventionally defined correlations, such as those examined in PN. Even when spanning clusters (spanning the radar swath) are removed from the sample, the average size does not decrease above the

critical point, likely associated with inhomogeneity in the water vapor field. Clusters are fairly compact in the interior, as expected from meteorological observations (Houze 2004). The relationship between cluster size and radius of gyration supports this, that is, large holes are rare. For values of w near and above criticality, which account for most of the large clusters, the cluster generally exists in a dryer environment, with a negative w -gradient from the center outward. This suggests gradient percolation as a prototype model for the behavior of the cluster boundary. The robust scaling prediction from gradient percolation, an accessible hull dimension of $4/3$, was found to hold, in approximate agreement with perimeter estimates in previous studies (Lovejoy 1982; Cahalan and Joseph 1989; Mapes and Houze 1993; Benner and Curry 1998). An implication is that area-perimeter relations for cloud clusters may be largely independent of the physical processes involved. This weakens the case for model validation via comparison of area-perimeter relations (Siebesma and Jonker 2000).

Overall, these results support the usefulness of considering geometric aspects of mesoscale phenomena in terms of very simple models, provided the change in properties across the transition to strong convection is taken into account, here seen as a function of water vapor. Several statistical properties of the clusters are common to clusters in many other physical systems. This is a reflection of universality in critical phenomena and emphasizes the broad applicability of associated results.

Such coarse-grained knowledge can complement studies that focus on the particular physics of convective processes by providing prototypes or null hypotheses for certain features of the complex behaviour, such as those mimicked by percolation with a probability dependent on the precipitable water. Of course, this must be placed in context with studies of mesoscale physics: for instance, the clusters are seen here to depend strongly on precip-

itable water, but the water vapor field in turn depends strongly on the convection, (e.g. Gamache and Houze 1983). Finally, we note that the scale-free range in the cluster size distribution near critical water vapor values extends across most of the range that can be examined with the TRMM radar resolution and swath width. Two traditional definitions of the mesoscale (Houze 1993; Mohr and Zipser 1996) here would imply cluster sizes greater than 500 km^2 and 2000 km^2 , but this size falls well within the scale free range – features as small as a few $5 \times 5 \text{ km}$ boxes appear to be part of the same scaling behavior. It may be worth working toward redefining the mesoscale range to reflect this.

Acknowledgments.

This work was supported in part by the National Science Foundation grant ATM-0645200, National Oceanic and Atmospheric Administration grant NA05OAR431-1134 (JDN and OP) and NA07OAR431-0214 (SN) and the Guggenheim Foundation (JDN). DN thanks J. L. Lin for asking what the PN results imply for cluster size distributions. OP would like to thank G. Pruessner, M. Gastner, and B. Oborny for helpful discussions on a related problem in ecology. We thank B. Stevens for discussions.

REFERENCES

- Barenblatt, G. I., 1996: *Scaling, Self-similarity, and Intermediate Asymptotics*. Cambridge University Press.
- Benner, T. C. and J. A. Curry, 1998: Characteristics of small tropical cumulus clouds and their impact on the environment. *J. Geophys. Res.*, **103 (D22)**, 28 753 – 28 767.
- Bernard, D., G. Bofetta, A. Celani, and G. Falkovich, 2006: Conformal invariance in two-dimensional turbulence. *Nature Phys.*, **2**, 124–128.
- Bretherton, C. S., M. E. Peters, and L. E. Back, 2004: Relationship between water vapor path and precipitation over the tropical oceans. *J. Clim.*, **17**, 1517–1528.
- Cahalan, R. F. and J. H. Joseph, 1989: Fractal statistics of cloud fields. *Mon. Wea. Rev.*, **117**, 261 – 272.
- Cardy, J., 2005: SLE for theoretical physicists. *Ann. Phys.*, **318**, 81–118.
- Cheng, C.-P. and R. A. J. Houze, 1979: The distribution of convective and mesoscale precipitation in gate radar echo patterns. *Mon. Wea. Rev.*, **107 (10)**, 1370–1381.
- Cotton, W. R. and R. A. Anthes, 1989: *Storm and Cloud Dynamics*. Academic Press.
- Fortunato, S., 2002: Site percolation and phase transitions in two dimensions. *Phys. Rev. B*, **66**, 054 107.

- Gamache, J. F. and R. A. J. Houze, 1983: Water budget of a mesoscale convective system in the tropics. *J. Atmos. Sci.*, **40**, 1835 – 1850.
- Gouyet, J.-F. and M. Rosso, 2005: Diffusion fronts and gradient percolation: A survey. *Physica A*, **357**, 86–96.
- Grossman, T. and A. Aharony, 1986: Structure and perimeters of percolation clusters. *J. Phys. A*, **19**, L745 – L751.
- Hinrichsen, H., 2000: Non-equilibrium critical phenomena and phase transitions into absorbing states. *Adv. Phys.*, **49** (7), 815–958.
- Houze, R. A. J., 1993: *Cloud Dynamics*. Academic Press Inc, San Diego.
- Houze, R. A. J., 2004: Mesoscale convective systems. *Rev. Geophys.*, **42**, RG 4003.
- Houze, R. A. J. and C.-P. Cheng, 1977: Radar characteristics of tropical convection observed during gate: Mean properties and trends over the summer season. *Mon. Wea. Rev.*, **105** (8), 964–980.
- Kertész, J., 1989: Existence of weak singularities when going around the liquid-gas critical point. *Physica A*, **161** (1), 58–62.
- Kolb, M., 1990: Crossover from standard to reduced hull for random percolation. *Phys. Rev. A*, **41** (10), 5725 – 5727.
- LeMone, M. A., E. J. Zipser, and S. B. Trier, 1998: The role of environmental shear and thermodynamic conditions in determining the structure and evolution of mesoscale convective systems during TOGACOARE. *J. Atmos. Sci.*, **55**, 3493 – 3518.

- López, R. A., 1977: The lognormal distribution and cumulus cloud populations. *Mon. Wea. Rev.*, **105**, 865–880.
- Lovejoy, S., 1982: Area-perimeter relation for rain and cloud areas. *Science*, **216** (4542), 185 – 187.
- Lucas, C., E. J. Zipser, and B. S. Ferrier, 2000: Sensitivity of tropical west Pacific oceanic squall lines to tropospheric wind and moisture profiles. *J. Atmos. Sci.*, **57**, 2351 – 2373.
- Mapes, B. E. and R. A. J. Houze, 1993: Cloud clusters and superclusters over the oceanic warm pool. *Mon. Wea. Rev.*, **121**, 1398–1415.
- Mohr, K. I. and E. J. Zipser, 1996: Mesoscale convective systems defined by their 85-GHz ice scattering signature: Size and intensity comparison over tropical oceans and continents. *Mon. Wea. Rev.*, **124**, 2417–2437.
- Moloney, N. R. and G. Pruessner, 2003: Asynchronously parallelized percolation on distributed machines. *Phys. Rev. E*, **67**, 037701.
- Nesbitt, S., W. R. Cifelli, and S. A. Rutledge, 2006: Storm morphology and rainfall characteristics of trmm precipitation features. *Mon. Wea. Rev.*, in press.
- Peters, O. and J. D. Neelin, 2006: Critical phenomena in atmospheric precipitation. *Nature Phys.*, **2**, 393–396.
- Siebesma, A. P. and H. J. J. Jonker, 2000: Anomalous scaling of cumulus cloud boundaries. *Phys. Rev. Lett.*, **85** (1), 214–217.

- Sornette, D., 1994: Sweeping of an instability: an alternative to self-organized criticality to get powerlaws without parameter tuning. *J. Phys. I France*, **4**, 209–221.
- Stauffer, D. and A. Aharony, 1994: *Introduction to Percolation Theory*. Taylor and Franics, London.
- Tompkins, A. M., 2001: Organization of tropical convection in low vertical wind shears: The role of water vapor. *J. Atmos. Sci.*, **58**, 529 – 545.
- Wentz, F. J. and R. W. Spencer, 1998: Ssm/i rain retrievals within an unified all-weather ocean algorithm. *J. Atmos. Sci.*, **56**, 1613–1627.
- Williams, M. and R. A. J. Houze, 1987: Satellite-observed characteristics of winter monsoon cloud clusters. *Mon. Wea. Rev.*, **115**, 505–519.

List of Figures

1	Radar-derived precipitation rates conditionally averaged as a function of water vapor for four tropical regions. The pick-up is well described by a power law (see inset), as expected for a continuous phase transition. The inset uses the critical water vapor values, from PN (derived from microwave observations) to present the data in reduced coordinates. The horizontal axis displays the dimensionless reduced water vapor, $(w_c^i - w)/w_c^i$, where w_c^i denotes the critical water vapor in a given region i . The vertical axis is the precipitation rate in arbitrary units chosen to offset individual curves.	30
2	Frequencies of occurrence of water vapor values (in bins of 0.3mm) during the entire measurement period for the same tropical regions as in Fig. 1.	31
3	The mean cluster size as a function of column water vapor w for the four tropical regions. Average sizes are dominated by single-pixel clusters for low water vapor values and pick up dramatically, with large fluctuations, as the critical water vapor level is surpassed.	32
4	The radius of gyration of as a function of column water vapor w for the four tropical regions. For low water vapor values, the average radius is dominated by clusters consisting of one pixel ($r \approx 3$ km). Near the precipitation transition, clusters with larger radii emerge. Note that the average area is not trivially related to the average radius due to the triangular inequality, $(\sum_i r_i)^2 \leq (\sum_i r_i^2)$	33

5	The median radius of gyration versus the median cluster size. Vertical and horizontal bars range from 5 th to 95 th percentile in bins defined by the cluster size.	34
6	Rank of clusters as a function of cluster size (number of clusters larger than a given size in km ²) for various values of the centroid water vapor, shown for the western Pacific. For the most frequent water vapor values, the distribution has a scale-free range. Apparent exponents (log-log slopes) are close to the 2- <i>d</i> percolation value of $-\tau + 1 = -187/91 + 1$ for the rank distribution. . .	35
7	The probability density function for a randomly selected cluster to be of a given size (km ²). Normalization is over all water vapor values. We show data for the western Pacific for various water vapor values at the centroid of the cluster. Two extreme cases, $w^{\max} = 75$, and $w^{\min}=25$ are shown. These cases differ considerably from percolation-type scaling. For water vapor values in the critical region, however, a power-law with percolation exponent (-187/91) is an acceptable approximation to the data. We therefore cannot exclude the possibility that the non-trivial character of mesoscale convective cluster size distributions is a result of a percolation transition.	36

8 Double-logarithmic plot of the length of the accessible hull, h , versus a linear scale, here the square-root of the cluster size, \sqrt{s} . Data points are median values both for h and \sqrt{s} for each of the four regions. Vertical and horizontal bars span the 5-percentile to 95-percentile range in each bin. These are not error bars; large clusters are so rare that the percentiles coincide, despite the uncertainty being large here. The red straight line has slope $4/3$, corresponding to the prediction from gradient percolation; the blue line represents trivial scaling, corresponding to a perimeter of dimension 1. 37

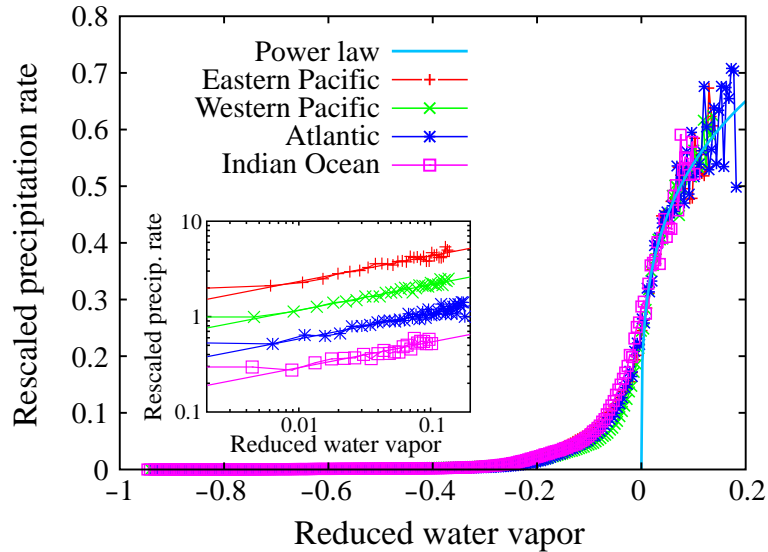


FIG. 1. Radar-derived precipitation rates conditionally averaged as a function of water vapor for four tropical regions. The pick-up is well described by a power law (see inset), as expected for a continuous phase transition. The inset uses the critical water vapor values, from PN (derived from microwave observations) to present the data in reduced coordinates. The horizontal axis displays the dimensionless reduced water vapor, $(w_c^i - w)/w_c^i$, where w_c^i denotes the critical water vapor in a given region i . The vertical axis is the precipitation rate in arbitrary units chosen to offset individual curves.

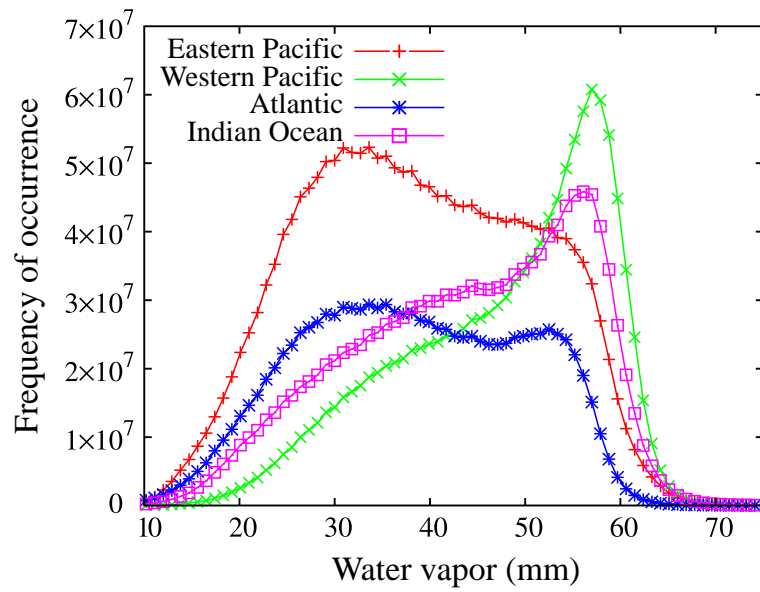


FIG. 2. Frequencies of occurrence of water vapor values (in bins of 0.3mm) during the entire measurement period for the same tropical regions as in Fig. 1.

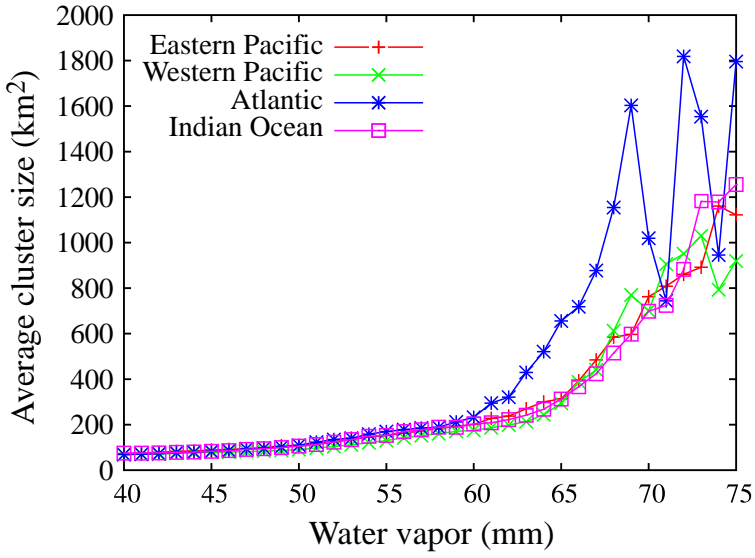


FIG. 3. The mean cluster size as a function of column water vapor w for the four tropical regions. Average sizes are dominated by single-pixel clusters for low water vapor values and pick up dramatically, with large fluctuations, as the critical water vapor level is surpassed.

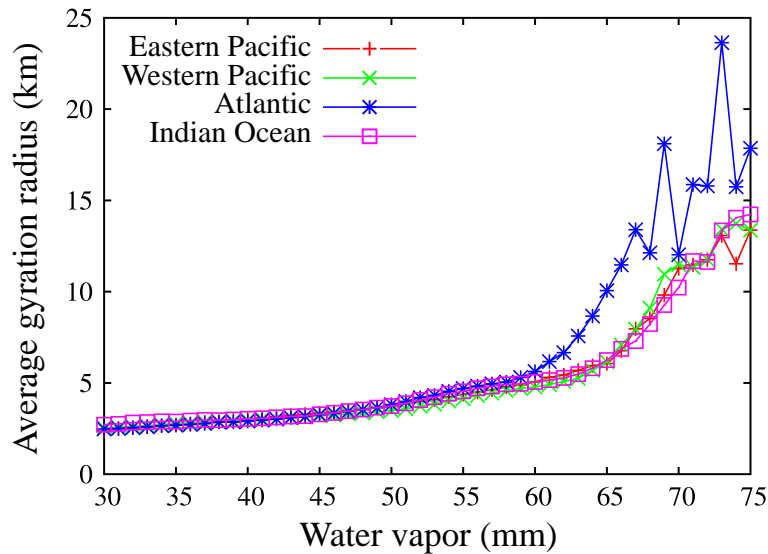


FIG. 4. The radius of gyration of as a function of column water vapor w for the four tropical regions. For low water vapor values, the average radius is dominated by clusters consisting of one pixel ($r \approx 3$ km). Near the precipitation transition, clusters with larger radii emerge. Note that the average area is not trivially related to the average radius due to the triangular inequality, $(\sum_i r_i)^2 \leq (\sum_i r_i^2)$.

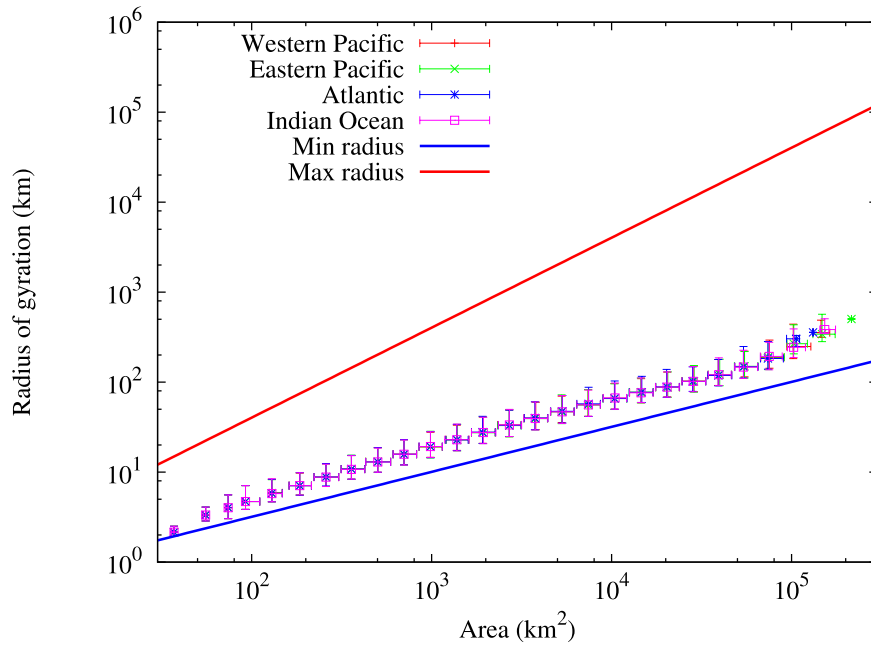


FIG. 5. The median radius of gyration versus the median cluster size. Vertical and horizontal bars range from 5th to 95th percentile in bins defined by the cluster size.

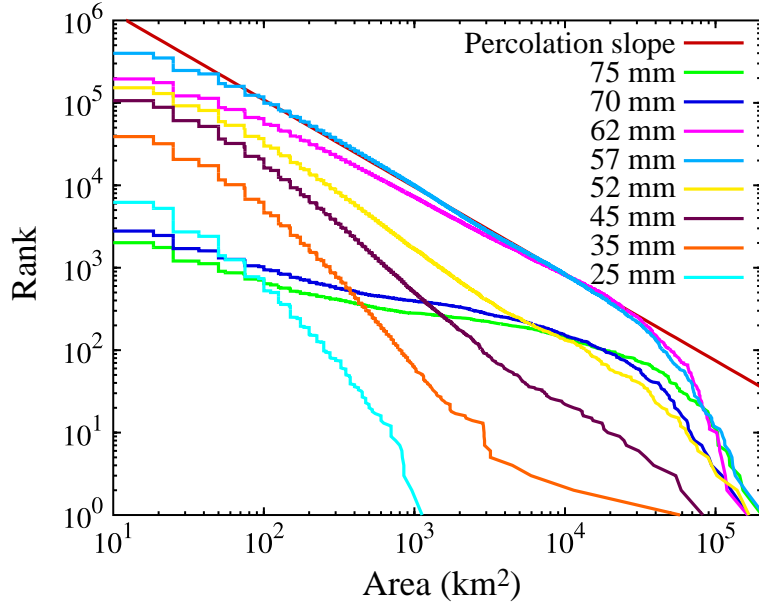


FIG. 6. Rank of clusters as a function of cluster size (number of clusters larger than a given size in km^2) for various values of the centroid water vapor, shown for the western Pacific. For the most frequent water vapor values, the distribution has a scale-free range. Apparent exponents (log-log slopes) are close to the $2-d$ percolation value of $-\tau + 1 = -187/91 + 1$ for the rank distribution.

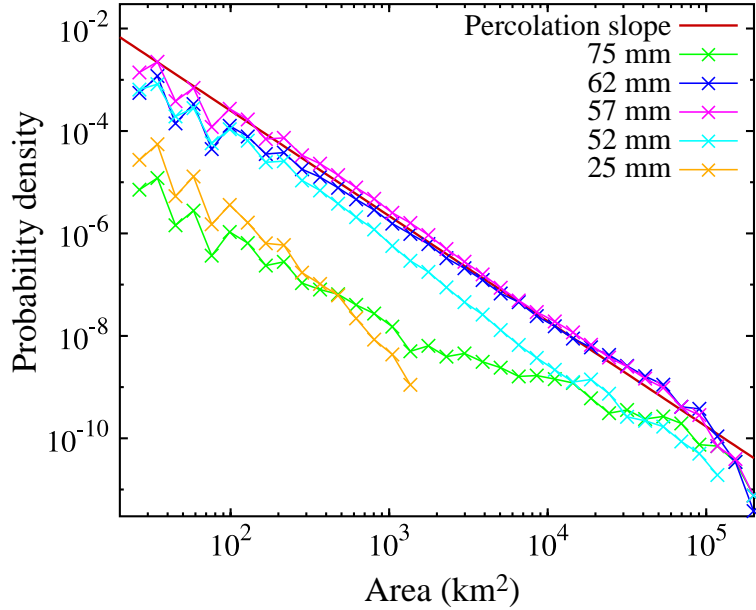


FIG. 7. The probability density function for a randomly selected cluster to be of a given size (km^2). Normalization is over all water vapor values. We show data for the western Pacific for various water vapor values at the centroid of the cluster. Two extreme cases, $w^{\max} = 75$, and $w^{\min} = 25$ are shown. These cases differ considerably from percolation-type scaling. For water vapor values in the critical region, however, a power-law with percolation exponent $(-187/91)$ is an acceptable approximation to the data. We therefore cannot exclude the possibility that the non-trivial character of mesoscale convective cluster size distributions is a result of a percolation transition.

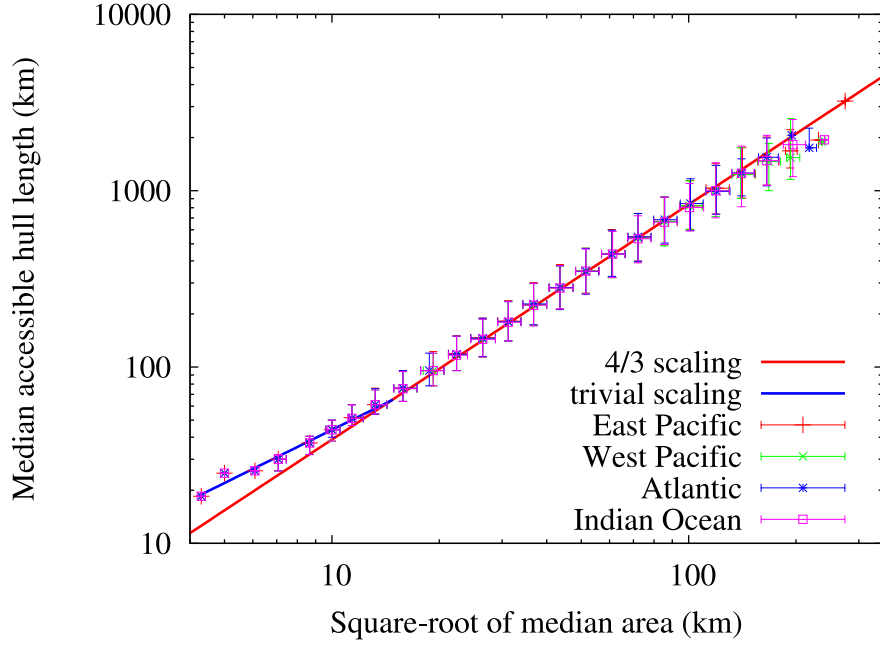


FIG. 8. Double-logarithmic plot of the length of the accessible hull, h , versus a linear scale, here the square-root of the cluster size, \sqrt{s} . Data points are median values both for h and \sqrt{s} for each of the four regions. Vertical and horizontal bars span the 5-percentile to 95-percentile range in each bin. These are not error bars; large clusters are so rare that the percentiles coincide, despite the uncertainty being large here. The red straight line has slope $4/3$, corresponding to the prediction from gradient percolation; the blue line represents trivial scaling, corresponding to a perimeter of dimension 1.